8-2017

Best Practices for Volume Flow Rate Measurements Using PIV at the Exit of a Turbulent Round Jet

Robert Schaap
Utah State University

BEST PRACTICES FOR VOLUME FLOW RATE MEASUREMENTS USING PIV AT THE

EXIT OF A TURBULENT ROUND JET

by

Robert M. Schaap

A thesis submitted in partial fulfillment
of the requirements for the degree

of

MASTER OF SCIENCE

in

Mechanical Engineering

Approved:

<table>
<tr><td>_____
Barton Smith, Ph.D.
Major Professor</td><td>_____
Geordie Richards, Ph.D.
Committee Member</td></tr>
<tr><td>
_____
Nicholas Roberts, Ph.D.
Committee Member</td><td>
_____
Mark R. McLellan, Ph.D.
Vice President for Research and
Dean of the School of Graduate Studies</td></tr>
</table>

UTAH STATE UNIVERSITY
Logan, Utah

2017

ABSTRACT

Best Practices for Volume Flow Rate Measurements Using PIV at the Exit of a Turbulent Round Jet

by

Robert M. Schaap, Master of Science

Utah State University, 2017

Major Professor: Barton Smith, Ph.D.
Department: Mechanical and Aerospace Engineering

Particle image velocimetry (PIV) is used to make volume-flow-rate measurements at the exit of a turbulent, round nozzle. The objective of this thesis is to assess a range of data acquisition and processing parameters. Data are acquired for Reynolds numbers between 10,000 and 100,000 for both two-component (2C) and stereo PIV. Spatial resolution has almost no effect on flow rate measurements. Images require preprocessing to remove reflections on the inside nozzle surface, which bias displacements to zero in those locations. Both 2C PIV and Stereo PIV were found to underestimate volume-flow-rate by approximately 2%. Several attempts to determine the cause of this error are made and discussed.

(51 pages)

PUBLIC ABSTRACT

Best Practices for Volume Flow Rate Measurements Using PIV at the Exit of a Turbulent Round Jet

Robert M. Schaap

Particle image velocimetry (PIV) is an optical flow measurement technique that is used to measure volume flow rate at the exit of a turbulent, round nozzle. The objective of this thesis is to determine how to best make this measurement. The quality of the measurement is affected by a range of data acquisition parameters and how data are processed. Measurements are made over a range of different flows using the two main types of PIV: Two Component (2C), which uses one camera, and Stereo, which uses two cameras, similar to human eyes. Previous work done for data acquisition and processing of PIV in general is found to apply. Different parameters are tested, evaluated, and discussed. Both 2C PIV and Stereo PIV were found to underestimate flow by approximately 2%.

CONTENTS

LIST OF TABLES

LIST OF FIGURES

CHAPTER 1

INTRODUCTION

Volumetric flow rate is a very common, yet somewhat complex, measurement that must be made in nearly all industries involving fluid flow. There are an assortment of different techniques used to make this measurement, some being more accurate than others. This work determines the feasibility and best practices for using Particle Image Velocimetry (PIV) for measurements of volume flow rate on a round geometry.

PIV is an optical flow measurement technique that uses a camera and a fluid seeded with particles to detect movement and provide instantaneous velocity fields. This method can provide two components of velocity over the entire field of view of the camera at an instant in time. A more complex version of the method, stereo PIV (SPIV), uses two cameras that view the same flow field from different angles, from which a third component of velocity can be extracted. This is an attractive option because it allows the measurement of velocity across the entire flow, which can then be integrated to determine volume flow rate.

This work finds the limitations of and the best methods for estimating volume flow rate from a round jet using PIV. Round nozzles are often used in engineering applications of flow handling for their ease of manufacture and well-characterized behavior. Challenges arise when dealing with round geometries because PIV data lie on a Cartesian grid, and thus do not conform to the contours of the geometry of interest.

Volume flow rate measurements at the exit of the nozzle are complicated by several factors. At the edges of the jet, there is a boundary layer between the fast and slow moving fluids where friction transfers momentum from the faster moving fluid to the slower moving fluid downstream of the nozzle exit. This increases the amount of fluid in the jet and consequently inflates the measured volume flow rate. For this reason, measurements should be taken as close to the nozzle exit as possible.

This work builds upon that of Cressall [1], which sought to find the ideal processing parameters

for a volume flow rate measurement in a rectangular geometry. From Cressall, we will use what was determined to be the "best case" processing for volume flow rate. This work however, will shift focus from processing parameters to methods of determining the volume flow rate of the round geometry. Additionally, we will study the impact of spatial resolution and calibration accuracy on the measurement.

CHAPTER 2

LITERATURE REVIEW

This chapter discusses the background and motivation of the work. Volume flow rate and how it is calculated are outlined. Next, the flow from the nozzle is described, along with Particle Image Velocimetry (PIV). After this, the method of data acquisition and reduction of the data are discussed. Finally, the measurement uncertainty and challenges involved with measuring volume flow rate using PIV are discussed.

2.1 Volume Flow Rate

Volume flow rate is defined as

$$Q = \int_{A_c} u \, dA_c \tag{2.1}$$

where A_c is the cross-sectional area of the plane and u is the local streamwise velocity. Two Component (2C) PIV only acquires data usable for flow rate calculation purposes on a line across the diameter of the nozzle exit. and therefore requires an assumption of symmetry around the center of the jet. For a flow rate calculation though a round jet, this assumption requires a modification to Equation 2.1, and becomes

$$Q_x = \pi \int_{-r}^{r} \bar{u}_i \cdot y \, dy \approx \sum (y_2 - y_1) \left[\frac{(\bar{u}_{i_2} \cdot y_2) - (\bar{u}_{i_1} \cdot y_1)}{2} \right] \tag{2.2}$$

or

$$Q_x = \pi \int_{-r}^{r} \bar{u}_j \cdot z \, dz \approx \sum (z_2 - z_1) \left[\frac{(\bar{u}_{j_2} \cdot z_2) - (\bar{u}_{j_1} \cdot z_1)}{2} \right] \tag{2.3}$$

These equations are for the XY and XZ planes respectively, and are a simple implementation of the trapezoidal rule combined with revolving the profile about the center of the jet to extract a volume flow rate.

Stereo Particle Image Velocimetry (PIV) determines the flow field on a regularly spaced square grid. In this work, the grid spans the entire exit of the nozzle. Thus, equation 2.1 becomes

$$Q_x \approx \sum_{j=1}^{N_z} \sum_{i=1}^{N_y} \bar{u}_{i,j} \, \Delta y \Delta z \qquad (2.4)$$

where $\bar{u}$ represents the mean velocity in the x-direction at each location and Δy, Δz are the vector spacing in the y and z directions.

2.2 Characteristics of a Jet

Turbulent jets are a type of free shear flow where the word "free" implies the flow is removed from any fixed surfaces and turbulence occurs because of the mean-velocity gradients [2]. Due to the short length of the nozzle used in this work, the flow will not be fully developed when it exits the nozzle and will have a near flat-topped velocity profile with a high rate of shear.

The flow near the jet exit has two main regions, the core and the shear layer. The core is the center of the jet that is not influenced by the surrounding, slower moving fluid. The core diminishes in size as the flow advances downstream. The shear layer is the interface between the core and the quiescent fluid characterized by a sharp velocity gradient and larger fluctuations in time.

In the shear layer, momentum is transferred from the fast moving fluid to the quiescent fluid. Momentum remains constant in the downstream direction and is determined by

$$M = \int_{A_c} \left(u^2 + \overline{u'u'} + \frac{p_s}{\rho} \right) \, dA_c \qquad (2.5)$$

where p_s is the gage static pressure and $\overline{u'u'}$ is the Reynolds normal stress. Both $\overline{u'u'}$ and p_s/ρ are smaller than the u^2 term, have opposite signs, and are generally ignored [3]. Reynolds stress is a measure of the mean fluctuations about the average velocity in turbulent flow, and is equivalent to the variance of the velocity in time. The result of momentum transfer is that fluid is entrained into the jet and increases the volume flow rate. This increase in volume flow rate is relevant to the present work in that it motivates acquisition as close to the exit as possible.

2.3 Particle Image Velocimetry

Particle Image Velocimetry is a non-intrusive, optical flow measurement technique that determines the velocity at discrete points on a plane. A laser sheet, which makes up the measurement plane, is used to illuminate tracer particles, which are imaged twice with a small, but known Δt. The images are subdivided into smaller sections called interrogation windows (IW). The most probable displacement for the particles inside each IW is determined using a cross correlation algorithm described below. Displacement can be converted from pixel units to millimeters using a scaling factor. This value is then divided by Δt to determine velocity. As described, the two components of velocity in the plane of the laser are returned, and this technique is therefore called 2C PIV.

Stereo PIV is an extension of 2C PIV that uses a second camera. Cameras are positioned with different viewing angles allowing the through-plane velocity component to be determined. This requires both cameras to be focused on the same position in the flow and a more complicated calibration [4].

PIV does not determine velocity by tracking the movement of individual particles, but uses a cross correlation to determine the most probable displacement of particles in an IW. The formula for a cross correlation is

$$C\left(x,y\right) = \sum_{i=-K}^{K} \sum_{j=-L}^{L} I\left(i,j\right) I'\left(i+x,j+y\right). \tag{2.6}$$

The pixel intensity values of each IW at time t and Δt are given by I and I' respectively. The K and L variables are dimensions in pixels in the x and y directions respectively, and are typically half of the IW size. Increasing the values of K and L increases the range of particle displacement detection with increased computational expense. Each combination of x and y are a potential displacement of the particles inside of the IW between images. Ideally, the value of $C(x,y)$ is a maximum when the x,y values match the actual particle displacement. The location of the peak indicates the most probable particle displacement. Figure 2.1 shows a correlation map with a single peak. The size of the peak is only important in distinguishing it from noise. As this is a statistical method, spurious velocity vectors occur and must be removed in a post-processing step [5].
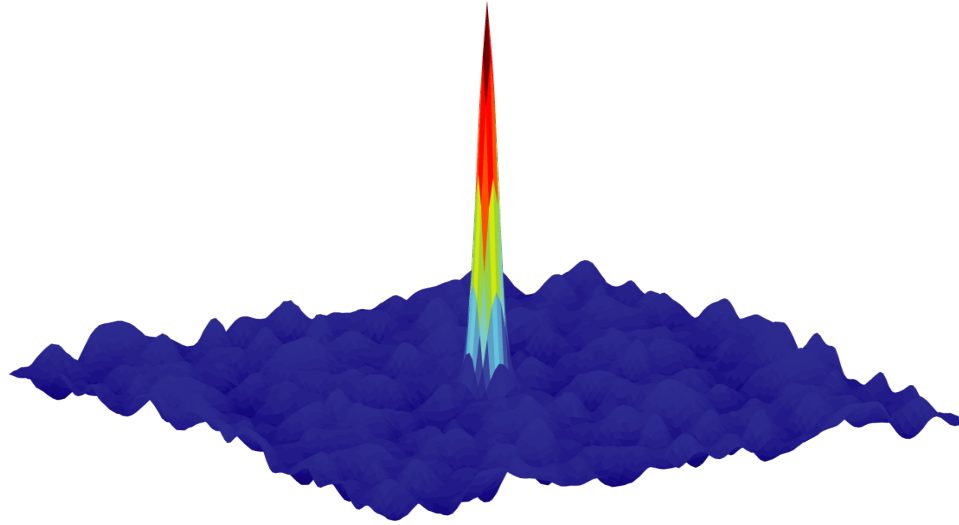
Fig. 2.1: Cross correlation map of two IWs. Peak location indicates the most likely particle displacement.

Since each IW produces a single vector, spatial resolution can be increased by overlapping IWs and/or by making them smaller. The minimum size of an IW has two primary constraints. First, sufficient particles must be present in both images so that the strength of the cross-correlation peak can be clearly distinguished from noise. Keane and Adrian [6] have shown that having eight particles per IW is sufficient to ensure a 95% valid detection rate. Second, particle displacement must be less than the IW size, generally limited to $^{1}/_{4}$ of its size. This prevents particles from moving far enough that they are not present in both IW's.

An iterative multipass scheme is often used, during which each pass produces a vector field that is used as a predictor for the next pass with the following step refining the measurement. After the first pass, the limitation of particle displacement and IW size is no longer necessary. This allows a higher spatial resolution by reducing the IW size on subsequent passes.

2.3.1 Data Acquisition Parameters

There are several data acquisition parameters that influence the accuracy of data collected. Guidelines for the follow data acquisition parameters are taken from Adrian [5].

Choosing a proper depth of focus (δ_z) for PIV images allows all particles within the measurement volume of the laser sheet to be in focus. Depth of focus is a function of the relative lens aperture ($f^\#$), image magnification (M_O), and the wavelength of the laser (λ) and is determined by

$$\delta_z \approx 4 \left(1 + \frac{1}{M_O}\right)^2 f^{\#2} \lambda. \tag{2.7}$$

Image magnification is the ratio of the camera sensor size to the Field Of View (FOV) size. Adrian [5] recommends a minimal magnification, M_{min} to avoid bias errors. The minimum magnification is a function of δ_z, λ, as well as particle diameter d_p and pixel pitch d_r,

$$M_{min} = \frac{2d_r}{\left(1.5\delta_z\lambda + d_p^2\right)^{1/2}} \tag{2.8}$$

for a given depth of focus. This is the smallest magnification that avoids bias errors due to the finite resolution of the recording medium.

Particle image size (d_τ) is the size, in pixels of particles illuminated by the laser. It is determined by a combination of the magnified particle diameter, the diffraction limited spot size of the particle using

$$d_\tau \approx \left(M_O^2 d_p^2 + d_s^2\right)^{1/2} \tag{2.9}$$

where d_p is the mean particle diameter and d_s is the diffraction limited spot size given by

$$d_s \approx 2.44 \left(1 + M_O\right) f^\# \lambda. \tag{2.10}$$

The tracer particles used are too small to optically resolve and light scattered from them appear as point sources. The image of a point object is always broadened by diffraction. The d_s terms represents this broadening and in many cases, $d_s \gg M_O d_p$.

Peak locking is a bias error where particle displacements trend towards integer values. A common source of peak locking is having particles images near or smaller than one pixel. This can be avoided by having $\frac{d_\tau}{d_r} > 2$ where d_r is the pixel pitch of the CCD sensor. Adrian [5] claims that random error is proportional to $\frac{d_\tau}{d_r}$, but more recent work by Timmins [7] show that random

error does not necessarily increase with particle image size. Timmins also showed that bias error is minimized when $d_\tau \approx 2.5$.

2.3.2   Processing Algorithm

A typical PIV algorithm can be broken into three steps: pre-processing of the images, vector calculation, and post-processing of the vectors. As many of the processing parameters affect different aspects of the PIV algorithm, this section describes the PIV algorithm specific to Davis 8.3.1 (which is used in this study) and its options. Exact implementation details for each processing step are covered in the DaVis Manuals [8, 9].

Pre-Processing

Pre-processing attempts to increase the signal to noise ratio (SNR) of particle images by removing contributions to pixel intensity from anything that is not a particle. To remove background noise that varies in intensity over time, such as laser reflections, a Butterworth filter was used. As reflections typically move slower than particles, this allows a high-pass filter to remove the laser light reflections. A Butterworth filter is chosen as a temporal high-pass filter for its flatness in its passband [10].

Particle intensity normalization applies a local particle intensity correction. It uses the minimum and maximum intensity values on a window defined by the scale length to normalize the intensity values of particle images. This homogenizes particle intensities and allows dimmer particles to contribute to the correlation peak.

Vector Calculation

Vector calculation is the most important process where the instantaneous vector field is determined. This process has a large number of options, which can be reduced to three different methods: CPU, GPU, and PIV+PTV. For this work, we will focus on the CPU method, which uses the CPU to calculate the correlation peak by exploiting properties of the convolution theorem and the Fast Fourier Transform. Implementation details are covered by Adrian [5]. This method is efficient and also tracks multiple correlation peaks. Secondary peaks can be used to determine if the primary

peak produces an invalid vector. Particle images are assumed to be Gaussian. This assumption implies that a Gaussian curve fit can be applied to the peak of the correlation and one point on either side in each dimension to find sub-pixel displacements. This process is done independently in the y and z directions [5].

The method used is an iterative, multipass scheme where the user chooses the size, weighting, overlap, and number of passes. The accuracy, spatial resolution and dynamic range improvements of a multi-pass scheme are well-established [5] and are not discussed here. Each pass produces an estimate of the vector field that is then used to deform the second PIV image of each pair. A perfectly known vector field with no through-plane motion should cause the first image to be a copy of the second image. Additional passes use the deformed images to produce vector fields that are used to correct the previous pass vector field. In addition to the IW options discussed above, there are several multipass options as well as multipass post-processing, where spurious vectors are identified and removed before deforming the images.

Post-Processing

The final step in a PIV algorithm is post-processing, where spurious vectors are identified and removed. The two methods to identify spurious vectors for this work are a median filter and Q-ratio. The median filter works by computing a median vector from a group of neighboring vectors and comparing the middle vector with this median vector plus or minus deviation of the neighboring vectors. This is done independently for each component of velocity and can be done iteratively.

The Q-ratio, which is not related to the Q used to define volume flow rate, is the ratio of the two largest correlation peaks. This value can be useful in determining if the highest peak is the actual displacement of the particles in a given IW. Q-ratio criteria removes a vector if the Q-ratio for an IW is not larger than the specified value. Typical values range from 1.3 to 3.0, where smaller values are more conservative, and larger values are more aggressive.

2.4 Measuring Volume Flow Rate

Before volume flow rate could be evaluated, the validity of the axisymmetric assumption had to be confirmed, along with the expected behavior of the flow. This was done by acquiring Stereo

PIV data across the entire jet exit at once, making it easy to see any abnormalities in the flow. Once these steps were taken, data was acquired with both 2C and Stereo PIV, which each have their own advantages and disadvantages. These challenges will be described in the following sections.

2.4.1   2C PIV

Volume flow rate from 2C PIV will be determined by acquiring data at two different locations and orientations as shown in Fig. 2.2. These orientations are limited by the geometry of the water tunnel walls as well as the fact that the flow on these planes should be axisymmetric with minimal through-plane motion. We believe no useful information would be obtained in acquiring data in planes that do not pass through the center of the nozzle. Since laser beams are not uniform throughout, the thickness of the sheet, and thus the extent of averaging in the direction normal to the laser sheet, changes in the span of the nozzle.

2.4.2   Stereo PIV

For Stereo PIV, fluid flow can be measured across the entire exit of the nozzle as shown in Fig. 2.3. Because the laser sheet has finite thickness, fluid downstream of the nozzle exit is entrained and included in the measurement, increasing the volume flow rate. This is shown schematically in Fig. 2.4 where the measurement volume is defined by a Gaussian laser sheet. Fluid entrainment starts at the exit plane of the nozzle, which is inside of the measurement plane.

Stereo measurements require two cameras that each view the laser sheet at a unique angle. Adrian and Westerweel [5] reported that increasing the angle between cameras increases the measurement sensitivity of stereo PIV to through-plane motion. We adopt their definition of θ as the angle between the optical axes of the imaging lenses with respect to the normal of the light sheet plane. The angle between cameras is therefore 2θ. Adrian and Westerweel also state that for values of θ between $30°$ and $45°$ the ratio of the mean random error amplitude in the through-plane component $\left(s_{\Delta x}\right)$ and the mean random error amplitude in the in-plane component $\left(s_{\Delta y}\right)$ is approximated by

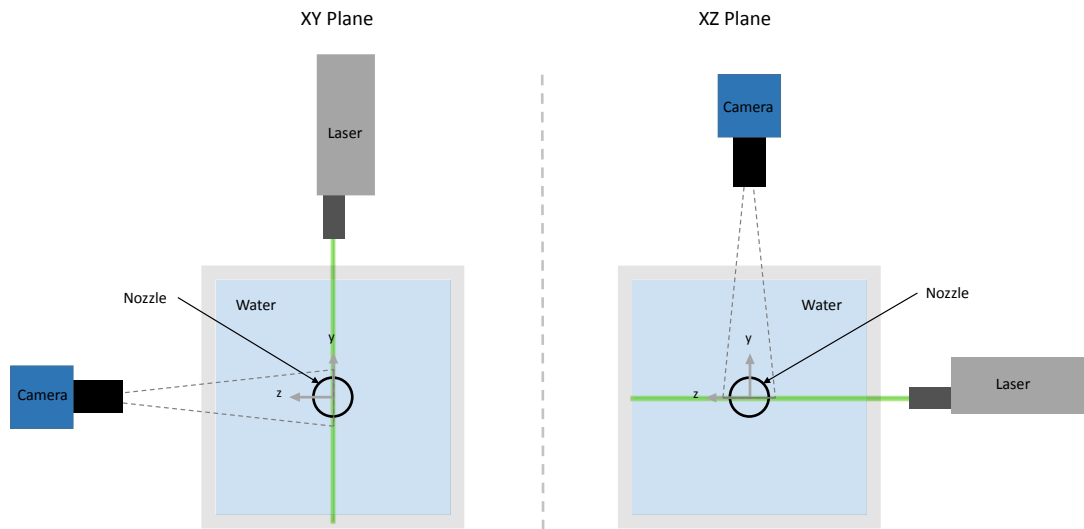Fig. 2.2: Cross section view of water tunnel illustrating the 2C PIV setups. Measurements were made in the 'XY' and 'XZ' planes at $z = 0$ and $y = 0$ respectively such that both planes intersect the center of the nozzle.
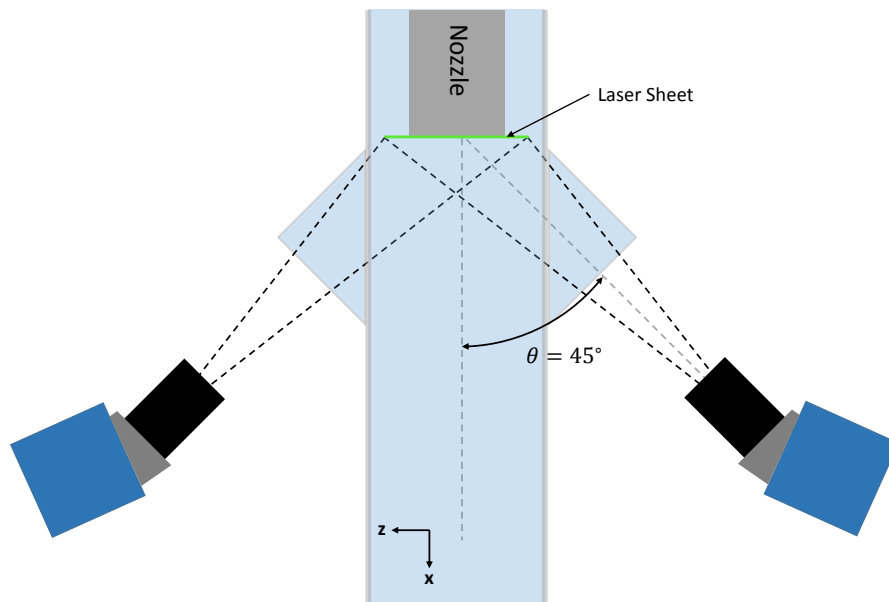

Fig. 2.3: Camera orientation for acquisition of Stereo PIV data. Two cameras view the nozzle from different angles, while the laser sheet is oriented such that it covers the entire exit of the nozzle.

$$\frac{s_{\Delta x}}{sa_{\Delta y}} \approx \left(\tan \frac{\theta}{2}\right)^{-1} \tag{2.11}$$

A plot of this function is shown in Fig. 2.5. Values of $\theta > 45°$ have not been reported as extensively, and the behavior of this trend beyond this range is unknown. If, however, the same trend were to continue past the range of study, this would suggest that the ratio becomes smaller than unity. In an effort to minimize the largest contributors to error, a value of $\theta = 60°$ will be tested and evaluated.

To calculate the three components of velocity, images from each camera are mapped (dewarped) onto the measurement plane. A calibration plate providing many known x, y, z locations is used to form the calibration map. Ideally, particles from both images will be mapped to the same location, but any errors in the mapping procedure will cause a mismatch between the two vector fields. A common error occurs when the calibration plane is not aligned with the measurement plane. Figure 2.6 shows a shift of the measurement plane relative to the calibration plane. When the images are dewarped to the calibration plane, this creates a disparity in the particle location between the two cameras [11].

To correct for misalignment between the calibration and measurement planes, a second calibration step is performed. This second step is called self-calibration and is described by Wieneke [12]. A disparity vector map is determined by performing a correlation between two dewarped images acquired at the same time. Because both images are acquired at the same time, any particle disparity between the two images is a misalignment between the measurement plane and calibration plane.

Performing an accurate self-calibration has been shown to be vital for high-quality stereo PIV data [13]. Volume flow rate measurements inside of a pipe done by van Doorne and Westerweel showed that small misalignments between the laser sheet (measurement plane) and calibration plane can cause significant errors in the estimation of velocity, particularly in regions of sharp gradients [14]. The present results confirm that an accurate calibration and self-calibration are both crucial to measurement of volume flow rate.
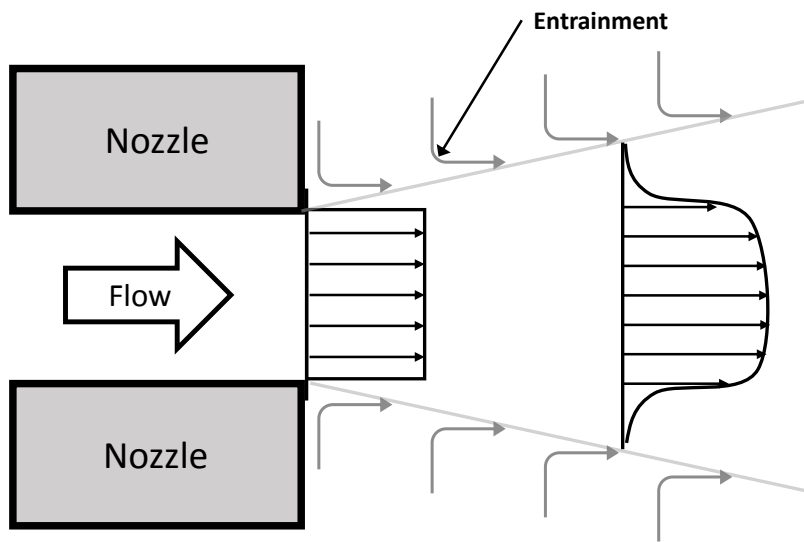
Fig. 2.4: Cross section schematic of a round nozzle showing how quiescent fluid is entrained by the moving fluid thus introducing error that grows with downstream distance.
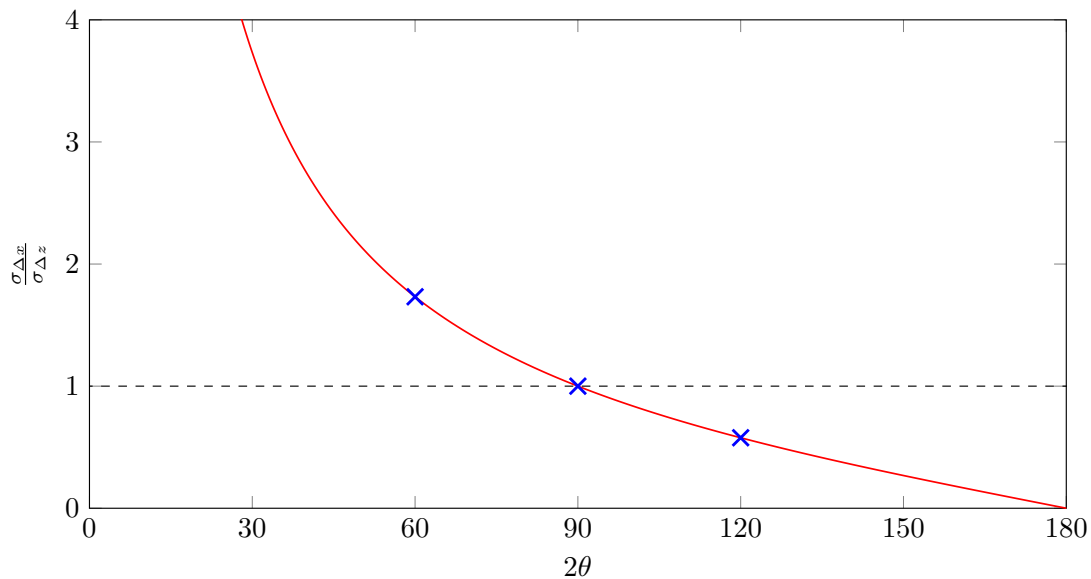
Fig. 2.5: Ratio of the mean random error in the in plane component to the through plane component vs. camera angle. Marks represent the values tested in this work.
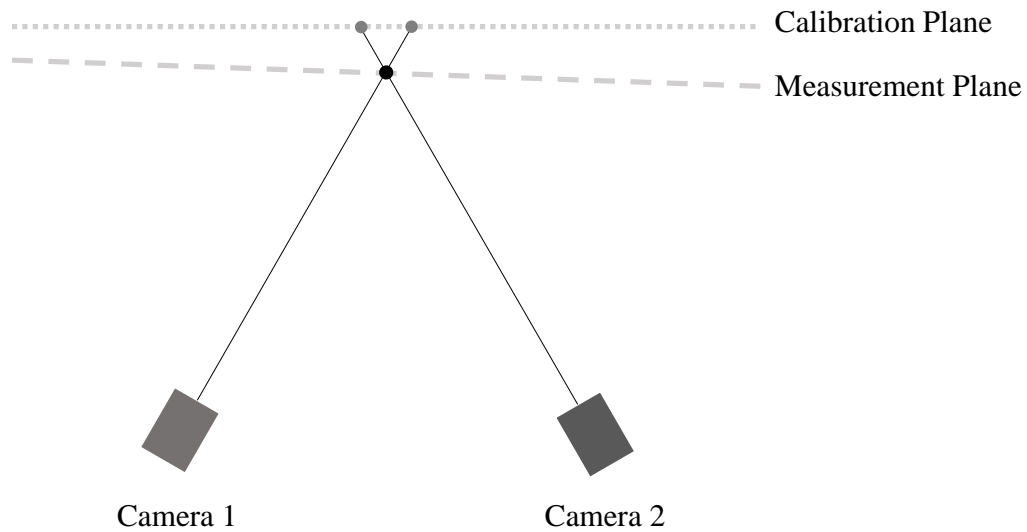
Fig. 2.6: A common stereo PIV calibration error occurs when the calibration plane and the measurement plane do not perfectly align. A shift of the calibration plane toward or away from the cameras will cause the same particle to appear in two different locations in the two views.

2.4.3 Calculating Volume Flow Rate

The output of PIV is an evenly spaced vector field, with each vector being representative of the flow at that location. For 2C PIV, the nozzle is assumed to be axisymmetric and the two profiles from the two orientations shown in Fig. 2.2 will be integrated independently and compared. Error from these will be determined by comparing the value with a high-accuracy flow meter, which will be considered the "ground truth" measurement.

For Stereo PIV, Eq. 2.4 can be used to calculate Q where Δy and Δz are the vector pitch in their respective directions. Stereo PIV presents a special challenge when applied to non-rectangular geometry because the data do not conform to the boundaries as shown in Figure 2.7. The difficulty is distinguishing between vectors that are inside and outside of the nozzle. It can be seen that some interrogation windows will straddle the edge of the nozzle, which leaves room for interpretation of which vectors contribute to the overall flow. Different methods of determining this will be tested and evaluated for volume flow rate calculation accuracy. Again, the calculated value will be contrasted with the value from the "ground truth" flow meter, and provide the error of the calculated value.

2.4.4 Volume Flow Rate Uncertainty

We use the Taylor Series Method for propagation of the velocity uncertainties to the for volume flow rate. Assuming no correlated uncertainties, the total uncertainty of Q can be expressed as

$$U_Q^2 = \sum_{i=1}^{J} \left(\frac{\partial Q}{\partial X_i} \right)^2 s_{X_i}^2 + \sum_{i=1}^{J} \left(\frac{\partial Q}{\partial X_i} \right)^2 b_{X_i}^2 + 2 \sum_{i=1}^{N-1} \sum_{k=i+1}^{N} \frac{1}{N} \frac{1}{N} b_{X_i X_k} \qquad (2.12)$$

where Eq. 2.4 is the data reduction equation for Q, s is the random uncertainty, and b is the bias uncertainty. The final term is the correlated bias uncertainties.

PIV measurement error has been extensively investigated using theoretical modeling [15], Monte Carlo simulations [16], and experimentally [17]. Bias, or systematic, errors in PIV are typically caused by particle slip, calibration, and peak locking [5]. Random errors often depend on the algorithm being used.
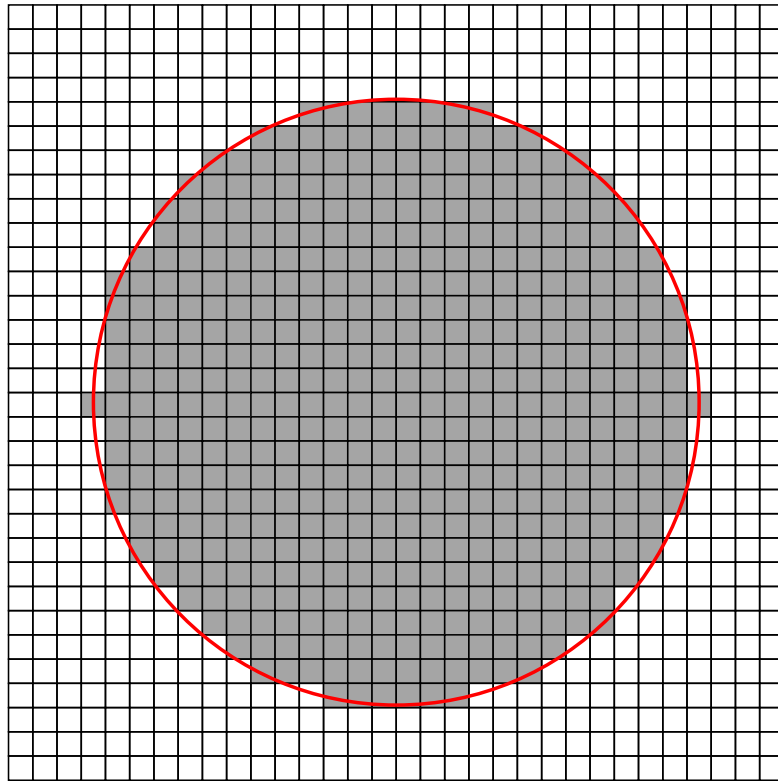

Fig. 2.7: Discrepancy between a round jet exit indicated by the red line and Stereo PIV data

Random uncertainty from the PIV calculation, which is likely the major source, is calculated by the DaVis software. Random uncertainty of the mean, from Coleman and Steele [18], is

$$s_{\bar{u}_i} = \frac{s_{u_i}}{\sqrt{n}}. \tag{2.13}$$

Random uncertainty which, by definition, quantifies errors with zero mean, is unlikely to have a significant effect on the total volume flow rate uncertainty as all data will be averaged in time and integrated in space.

Bias errors are not reduced under integration (e.g. averaging in time and space) and are expected to dominate the uncertainty of volume flow rate. When propagating biases, it is important to consider whether the bias errors in the individual velocity values that are integrated to find volume flow rate are correlated to one another. If they are not, each velocity has a unique bias error, and the profile will appear "noisy". The values of $b_{X_i X_k}$ in Eq. 2.12 are all zero, and, as shown in [18],

$$b_Q = A \frac{b_V}{\sqrt{N}}, \tag{2.14}$$

where N is the number of points in the velocity profile that are to be integrated.

Since, as will be shown in Sec. 5.4 that the major bias source is the calibration target, and since the calibration target is involved in every velocity measurement, all velocity biases due to this source are correlated to one another. This means that $b_{X_i X_k} = b_{X_i} b_{X_k}$ and

$$b_Q/Q = b_V/V, \tag{2.15}$$

where b_V is the common bias uncertainty of each velocity measurement. In this case, the relative uncertainty of the volume flow rate is the same as the relative uncertainty of the velocity, and acquiring additional data points in space does not improve the result.

CHAPTER 3

EQUIPMENT

3.1 Test Facility

The water tunnel is a standard tunnel from ELD with modifications including a lengthened test section, a larger pump, and a filter for the seeding particles. The facility is shown in Fig. 3.1. It has a modular design allowing for different nozzles. Flow is driven by a centrifugal pump designed to deliver 370 GPM against a pressure of 11'6" of water, and powered by a 3HP TEFC 1800 RPM motor using 208-230V AC/3Φ/60Hz/5 amp service and controlled by a variable frequency inverter.
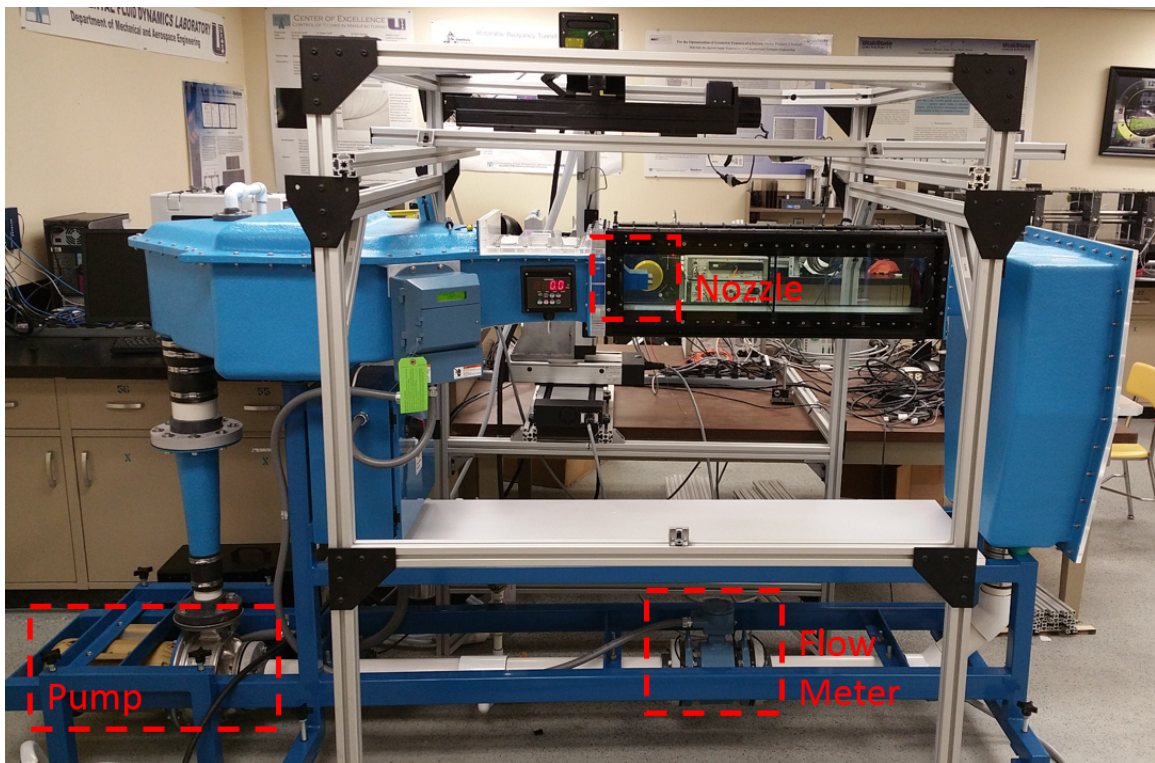

Fig. 3.1: Photo of Water Tunnel Facility used for this study. The jet nozzle, pump and flow meter are labeled.

3.2 Flow Meter

A high-accuracy magnetic flow meter manufactured by Rosemount Inc. model 8705 is located on the underside of the facility. This meter has an accuracy of $\pm 0.5\%$ of reading and is non-obtrusive. The meter serves as the "ground truth" measurement from which PIV measurements will be evaluated.

3.3 Nozzle

The round nozzle was designed in house, and is made out of 6064-aluminum. The contour of the inside surface was calculated by fitting it to a 5th order polynomial, which requires six boundary conditions. For this case, the conditions were: both the inlet and outlet ends have the first and second derivatives equal to zero, and the positions of each end were fixed. The nozzle was designed to have approximately a 20:1 inlet-to-outlet area ratio. The as-built diameter of the nozzle is 1.951cm. The contour is seen in Fig. 3.2.

It was found that raw aluminum surfaces in water tend to pit, especially with the presence of other metals that have liquid contact. To avoid this problem, the nozzle was anodized.

3.4 Camera

Cameras used were sCMOS cameras purchased from LaVision for the sole purpose of acquiring PIV data. These cameras have a resolution of 2560×2160 pixels, which provides sufficient spatial resolution. The bit depth of the cameras is 16, which means there are 2^{16} different intensity values that each pixel can have. This is desirable over smaller depth cameras for PIV because it allows the measurements to be less sensitive to the illumination of the particles.

3.5 Optics

When acquiring stereo data, cameras are viewing the nozzle at an angle. If no action is taken, the entire exit plane cannot be in focus at one time. To remedy this problem, we introduce a sheimpflug adapter, which allows the camera to move relative to the lens. This enables the camera to focus on the entire nozzle exit when viewing from an angle. An example of this is shown in Fig. 3.3, details of sheimpflug criteria are not covered in this work.
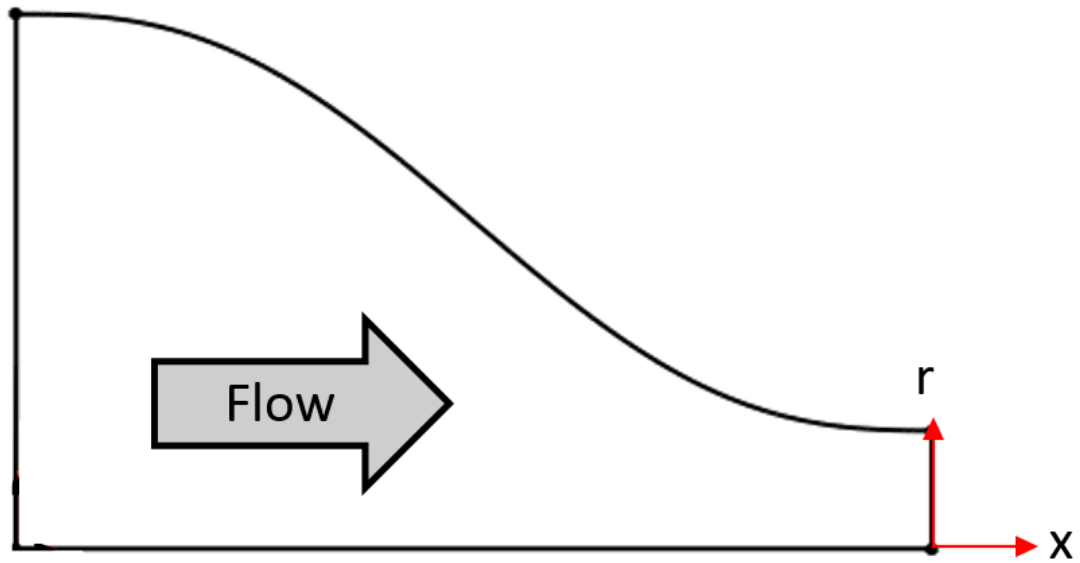
Fig. 3.2: Contour of the inside surface of the nozzle. The profile was revolved around the centerline.

Fig. 3.3: A Camera and lens attached to a scheimpflug adapter. This adapter allows the camera to move relative to the lens.

3.6 Laser

A dual cavity Quantel Evergreen laser was used for this experiment. It has a wavelength of 532nm. The two cavities allow the laser to fire two pulses very close together in time. Optics inside the laser are arranged such that these to beams are coincident with one another. The beams are passed through a cylindrical lens such that the beam spreads out into a sheet. This sheet constitutes

the measurement plane for PIV.

3.7   Calibration Plate for Stereo PIV

Stereo calibration is the process of mapping the images of each camera to physical coordinates. Since each camera is viewing the exit of the nozzle at a unique angle, there must be a well-defined calibration target that maps the physical coordinates the view of each camera.

For this experiment, a standard 058-5 two-plane calibration target was purchased from LaVision. This plate was modified to be used *in-situ* by drilling a hole such that the plate can be placed surrounding the nozzle exit, as shown in Figure 3.4.

Because the bulk direction of the flow is through the laser sheet, it is crucial that the plane-to-plane depth of the calibration target is well defined. The LaVision 058-5 target has a nominal plane-to-plane depth of 1mm, and a dot spacing of 5mm
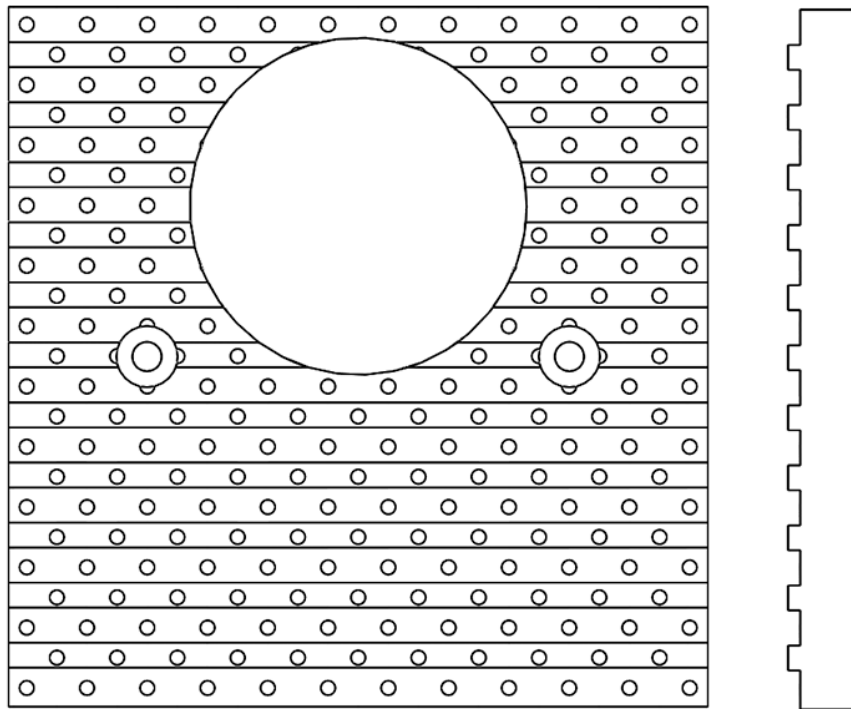
Fig. 3.4: LaVision calibration plate modified with a hole in the center that accommodates the jet nozzle.

3.8 Stereo PIV Setup

Cameras were mounted on either side of the test section at equal and opposite angles. The light must pass 3 different media (air, glass, and water) before it reaches the nozzle exit. If no action is taken to prevent it, a large amount of distortion occurs when looking at an angle through these media, due to differences in index of refraction. To remedy this situation, water-filled prisms were placed on the outside of the water tunnel such that the camera lens was oriented perpendicular to the face of the prisms. This minimizes index of refraction issues, which effect can be seen in Fig. 3.5.

3.8.1 Stereo Calibration

Calibration requires both cameras to be viewing an object that has many known locations in

Fig. 3.5: Nozzle and calibration plate viewed with out (top) and with (bottom) prism.

physical space. For this experiment, the calibration procedure was accomplished by securing a calibration target to the front face of the nozzle. The front plane of th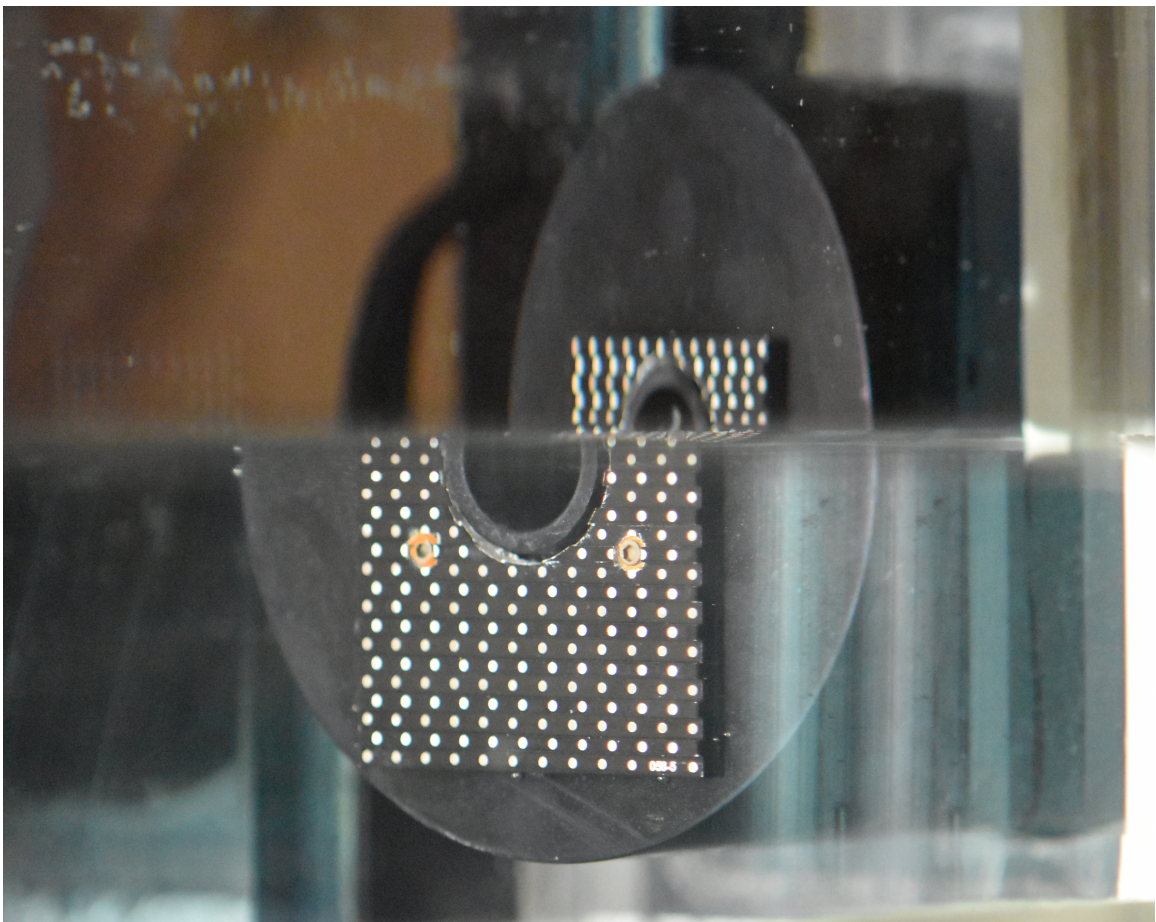e target was aligned with the exit of the nozzle, such that the distance between the calibration plane and measurement plane was minimized. During calibration, the calibration target occupied the entire field of view for each camera.

The portion of the target used for calibration was located below $(-y)$ the nozzle, and thus the cameras had to be translated in the positive y-direction to have the nozzle exit in view. This translation was accomplished with a Newport 281 Lab Jack, which has a travel range of 76mm. This jack was connected to an optical rail, which had a camera hanging on either side.

3.9 Facility Operation

3.9.1 Flow Control

The pump is controlled by a variable frequency inverter, which has a range of 0.5 - 60 Hz in increments of 0.1 Hz. The Reynolds number at each of the limits of the pump easily covers the range (10,000 - 100,000) of interest.

3.9.2 Particle Seeding

Tunnel was seeded using Sphericel® 110P8 hollow glass spheres. Particles were blended up with a small amount of water and Simple Green solution to break up surface tension. These particles were then injected with a syringe downstream of the nozzle. Particle density was estimated by DaVis which reports particle density in Particles per Pixel (PPP), the number of particles per IW can then be deduced by multiplying this number by the number of pixels in each IW.

CHAPTER 4

RESULTS

4.1 Facility Shakedown

Preliminary SPIV data was acquired at Re= $10,000$ and $100,000$ using the setup shown in Fig. 2.3 from which we conclude that the jet behaves as expected and is axisymmetric. SPIV was used so that data could be acquired across the entirety of the nozzle, and flow over the nozzle could be characterized, a diagram of this setup is shown in Fig. 2.3. No major problems were found during shakedown. A velocity profile of the preliminary data is shown in Fig. 4.1.
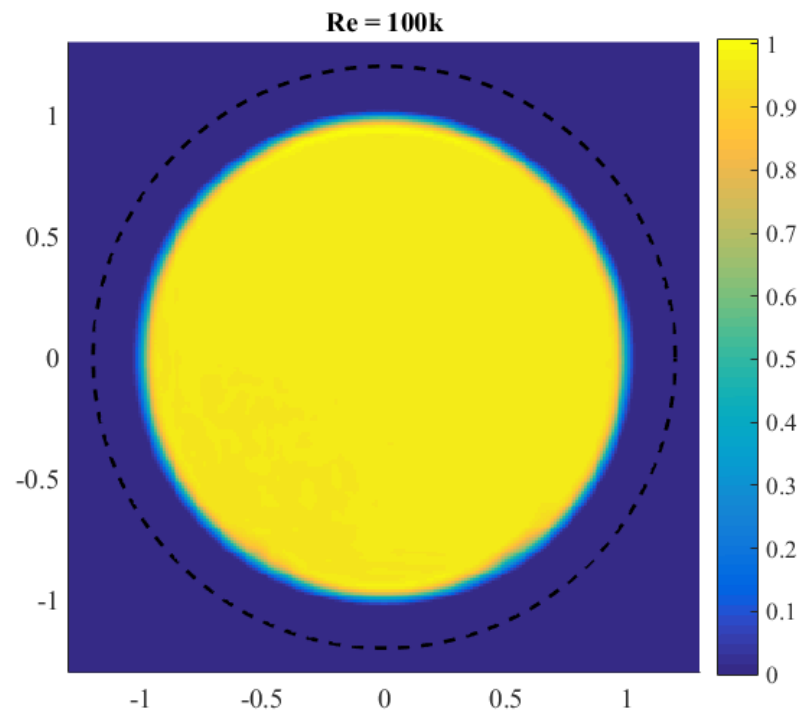

Fig. 4.1: Velocity contour plot for preliminary data.

4.2 Volume Flow Rate Measurements

4.2.1 2C PIV

Data were acquired at two different planes, XY and XZ. The resultant volume flow rate errors are shown in Table 4.1. The results consistently underestimated the volume flow rate by $\approx 2\%$.

4.2.2 Stereo PIV

Turbulent and laminar flows have very different shear rates, and as mentioned previously, PIV generally has trouble in areas of flow that have high rates of shear. The velocity profiles of the three different Re are shown in Figure 4.4. Values of the flow rate error are reported in Table 4.3.

A consistent negative bias of approximately 2% is apparent for both $45°$ and $60°$, but is a positive 1.5% for $30°$. Figure 4.5 shows that velocity profiles from different camera angles match well, with the exception of the $30°$ case. The discrepancy in the $30°$ data was found not to be representative of the actual flow. Evidence of this was noted in the centerline profiles shown in Fig. 4.6.

Self-calibration corrects for a mismatch between the measurement plane (laser sheet) and the calibration plane. However, disparity can exist for other reasons. In the present case, the translation of the cameras to change the field of view from below the nozzle (where calibration dots are present) to the nozzle can result in errors in the camera locations that cannot be corrected in self-calibration.

Table 4.1: Volume flow rate error from 2C PIV cases for two different planes and three different Reynolds Numbers. Negative values represent an underestimation of the value reported by flow meter.

Plane	Reynolds Number		
	$10,000$	$75,000$	$100,000$
XY	-3.13%	-2.01%	-2.16%
XZ	-1.56%	-1.14%	-1.07%

Table 4.2: Typical data acquisition parameters. The values reported are for $45°$ at Re $= 100,000$.

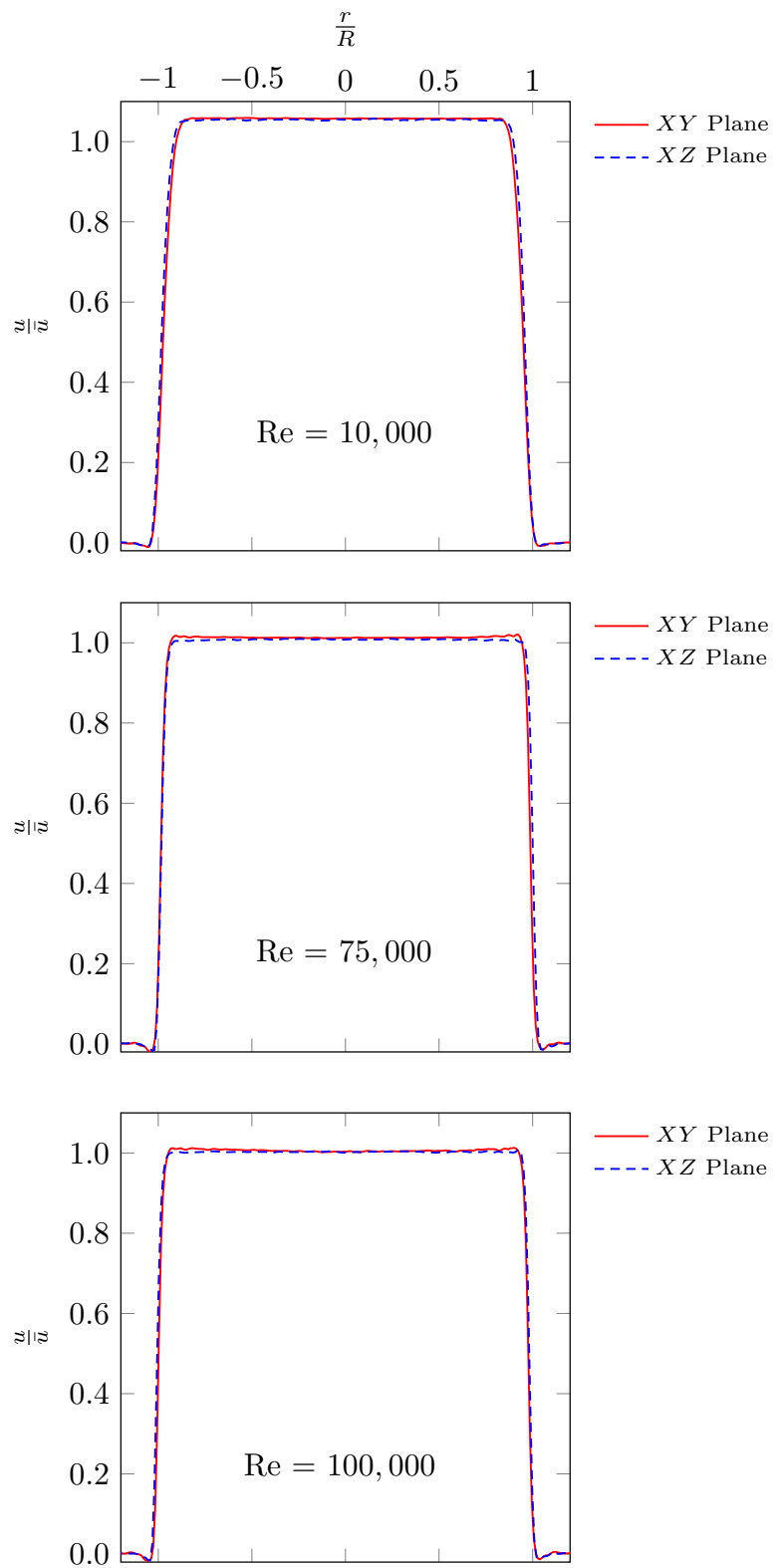|	
Particles Per Pixel (PPP)	0.005
Particle Size (pix)	2.1
Data Acquisition Rate (Hz)	2
Particle Displacement(pix)	4

Fig. 4.2: Two Component velocity profiles for different Reynolds number values.
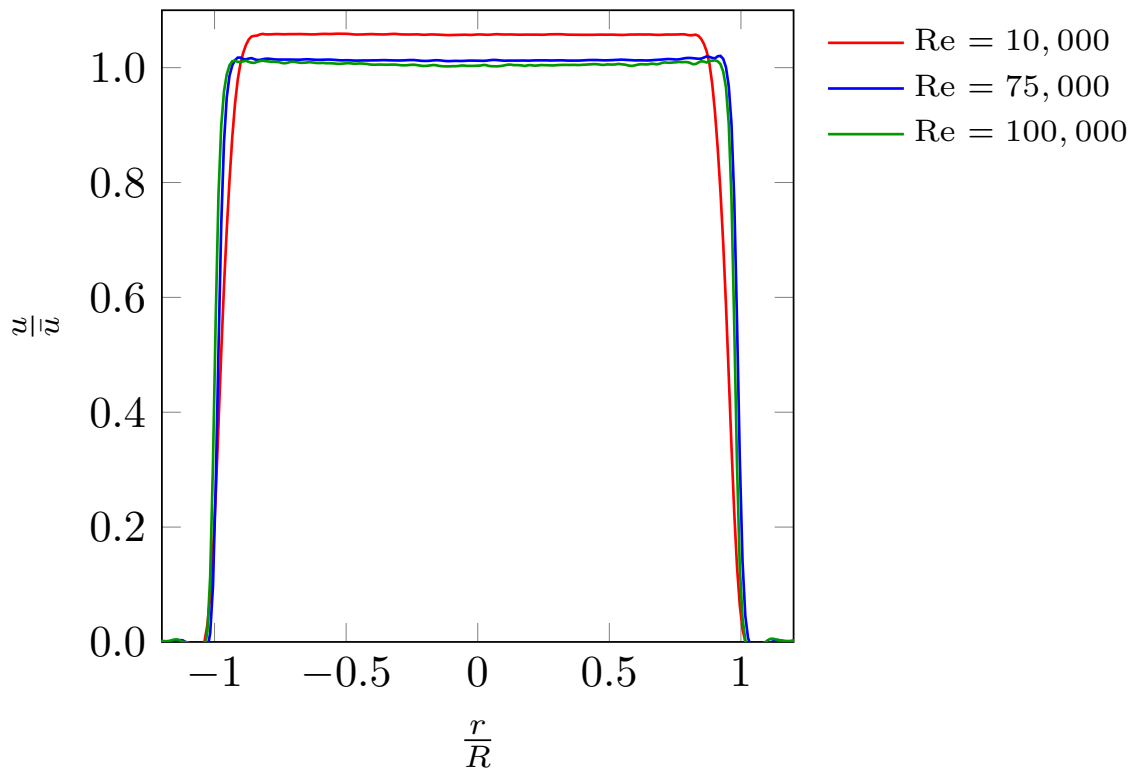
Fig. 4.3: Centerline velocity profiles from the XY plane for all Reynolds numbers at which data were acquired.
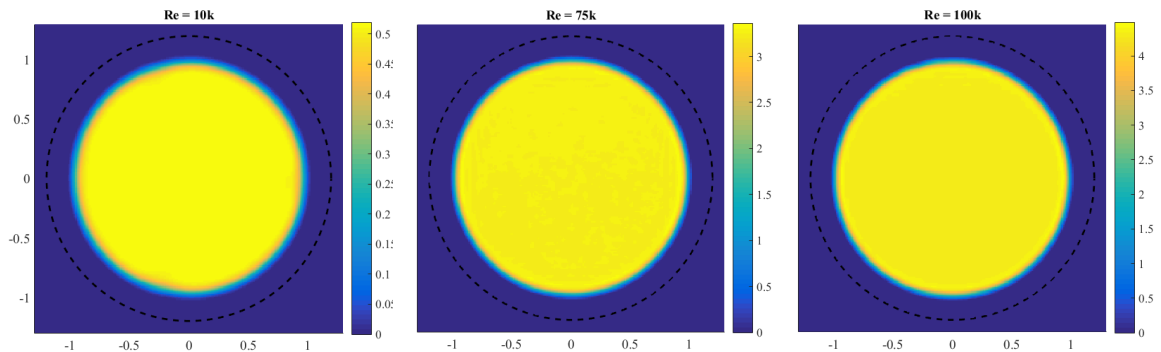
Fig. 4.4: Stereo velocity contour plots for different Reynolds numbers.

For instance, a rotation of the bean supporting the cameras around the x-axis causes one camera to move up while the other moves down, resulting in vertical disparity.

While self-calibration cannot correct for vertical disparity, a simple script from Cressall [1] can shift the images to remove a roughly uniform vertical disparity, shown in Fig. 4.7. If ver-

Table 4.3: Volume flow rate error for Stereo PIV for different Reynolds Numbers and angles of cameras.

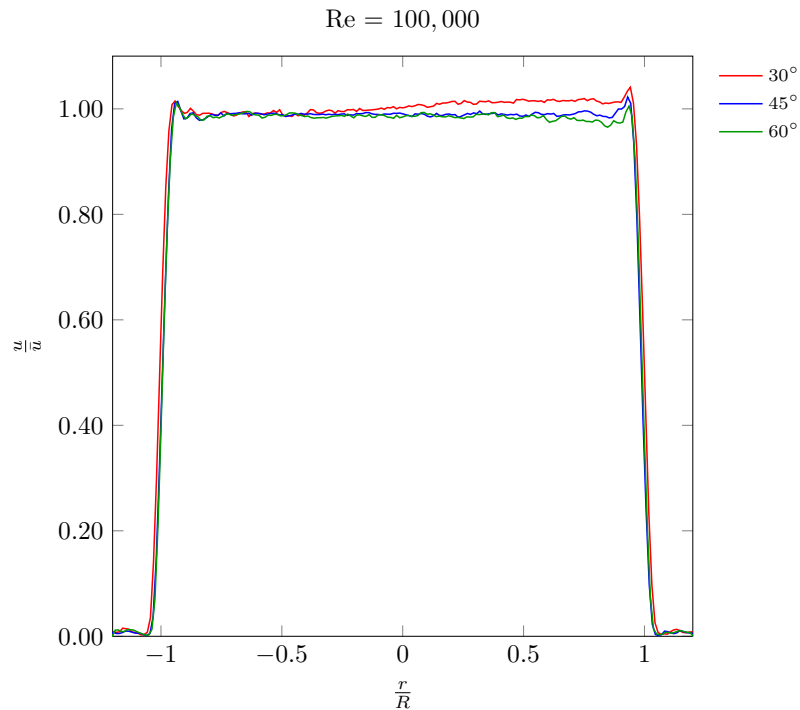| Prism Angle	Reynolds Number		
	10,000	75,000	100,000
30°	0.38%	1.48%	1.31%
45°	−3.02%	−1.90%	−1.95%
60°	−2.69%	−1.38%	−1.58%

Fig. 4.5: Centerline velocity profiles for Re = 100,000 from all stereo camera angles.

tical disparity is not removed, the resulting velocity contour will look similar to Fig. 4.8, which shows distortion of the nozzle exit plane in the vertical direction. We find that this results in larger measured volume flow rate due to the resultant larger flow area.

It is thought that for the 30° data, a random rotation of the camera beam around a different axis during translation caused the non-uniform vertical disparity shown in Fig. 4.9. This issue is most likely the result of either movement of the cameras relative to each other, or a parallelism error during translation of the cameras in the y-axis, which was within specification of the jack. Self-Calibration can account for simultaneous rotation of the cameras about the y and z axes and translations in the x-direction, but cannot correct any other movements. The coordinate system is
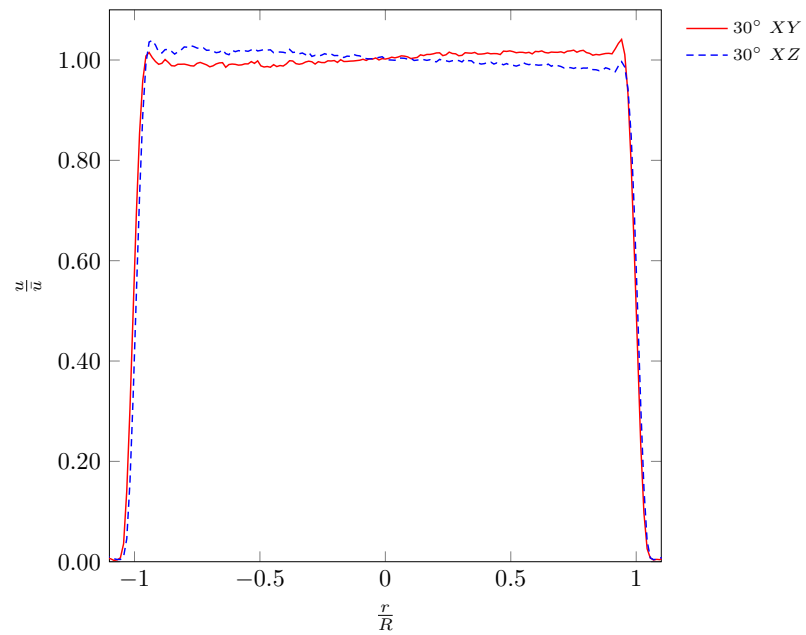
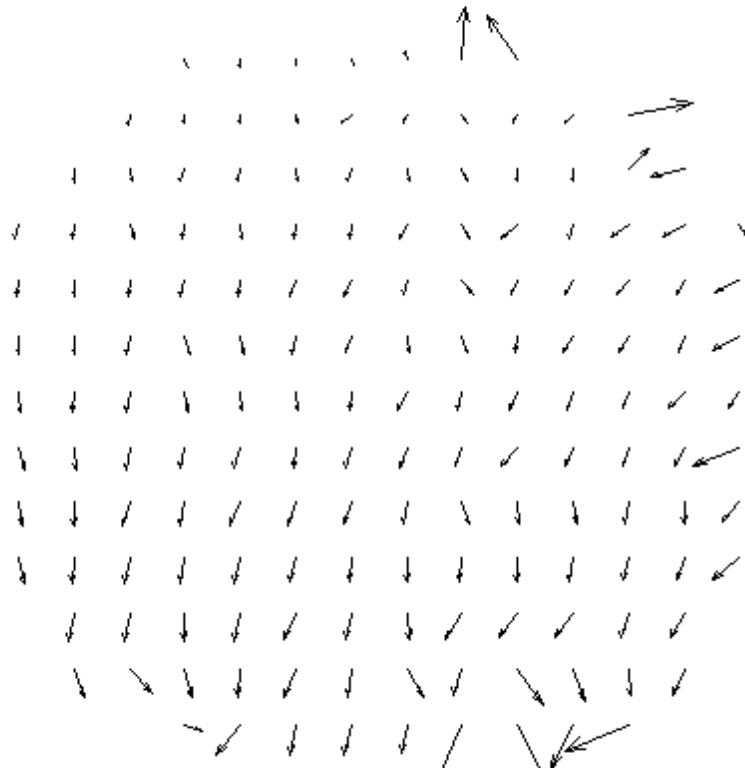Fig. 4.6: Centerline velocity profiles for 30° stereo angle.

Fig. 4.7: Disparity map with roughly uniform vertical disparity, which can be corrected.
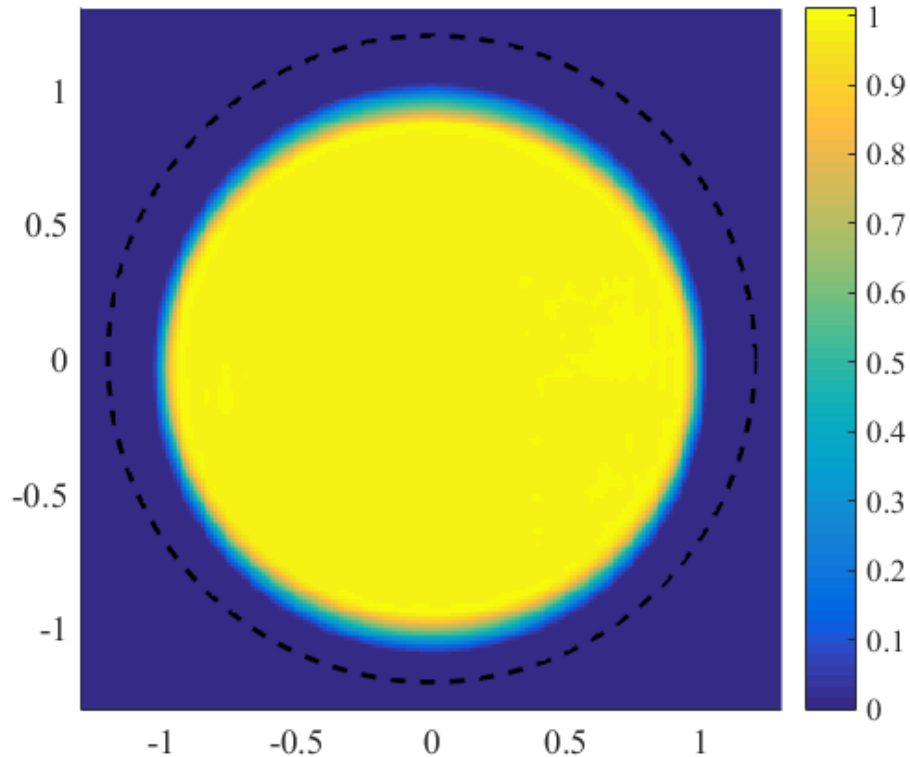
Fig. 4.8: Velocity contour of data that has vertical disparity. Profile appears stretched in the vertical direction.

shown in Fig. 4.10. Steps were taken to resolve the issue, but none of the attempts were successful, and therefore these data were deemed unusable. Results for this value of θ are inconclusive, and must be studied further.

We determine the effect of spatial resolution relative to the nozzle size by varying the size of the IW. This is important because in some cases, it may not be possible to achieve the desired resolution for a volume flow rate measurement, such as when the flow through several jet exits are to be measured at once. This was tested on a SPIV case where $Re = 100,000$ and $\theta = 45°$. We find that this parameter had almost no effect on the volume flow rate measurement, with very little deviation from an IW size from 16×16 to 128×128. This range of IW size corresponds to 314 and 39 velocity vectors respectively across the diameter of the nozzle. As shown in Table 4.4, spatial resolution has little impact on the volume flow rate using the methods described in this thesis (e.g. integrating beyond the nozzle dimension).
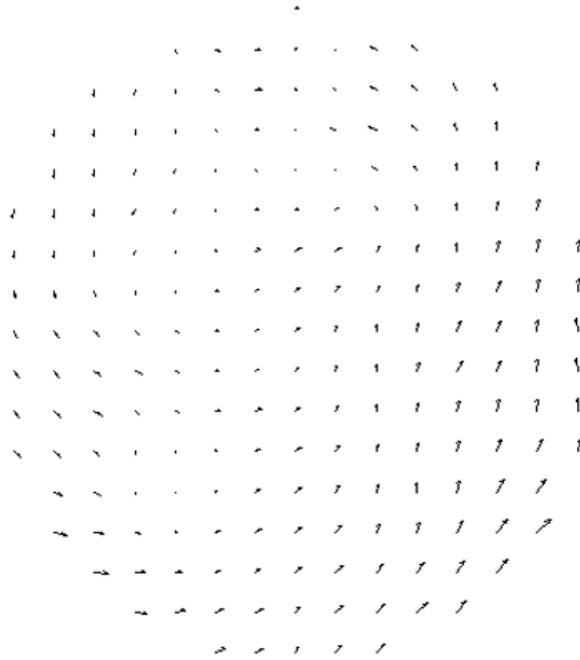
Fig. 4.9: Disparity map after self-calibration was performed on the 30° data. It is clear that the vertical disparity is not uniform and therefore the result of an unfixable movement of the cameras during translation.

To show the reason for the insensitivity to spatial resolution, centerline velocity profiles for this study are shown in Fig. 4.12. Large IW regions are shown to result in considerable smoothing of the profile and reduction in the measured rate of shear. However, since we integrate beyond the nozzle boundary, the flow rate is preserved under this smoothing. It is noted that for the smallest IW size, the measurement in the core of the jet is noisy. This result is expected because of insufficient particle density results in increased random error.
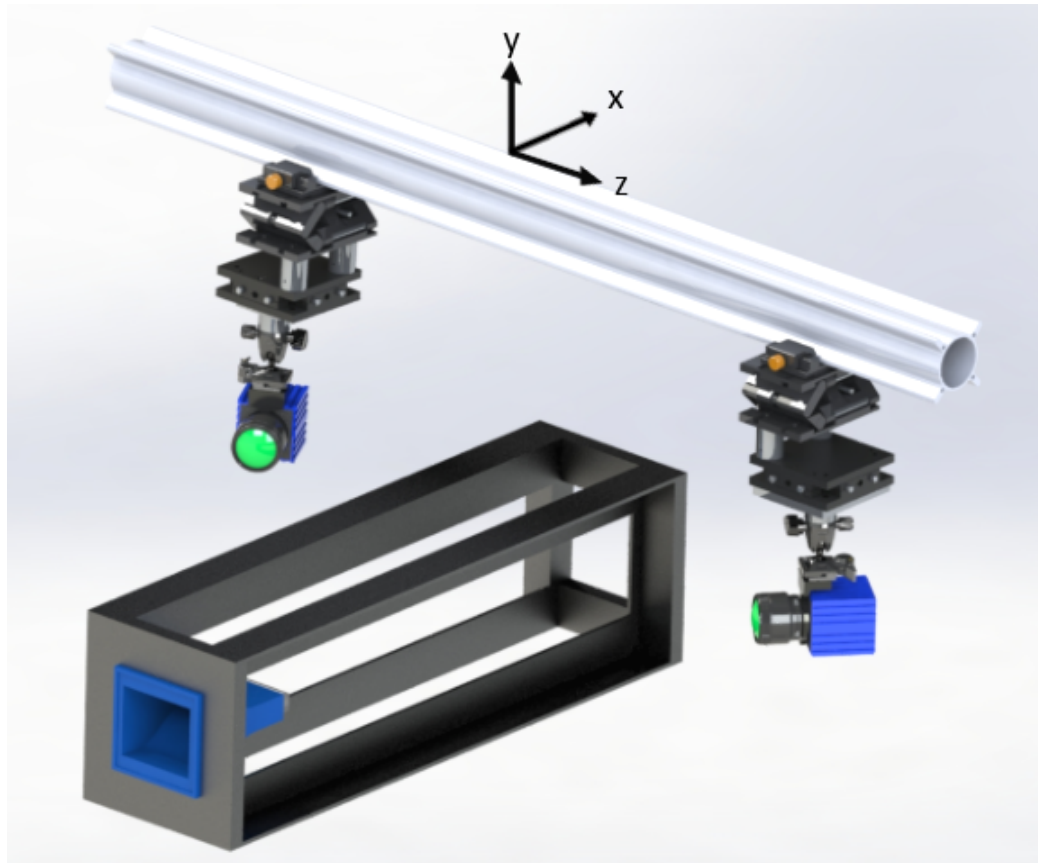
Fig. 4.10: Schematic drawing of the stereo set-up. Cameras are translated in the $+y$-direction after calibration. Translation stage has 3 mrad parallelism over the 76mm of travel.

Table 4.4: Volume flow rate error from Stereo PIV for different IW Size.

IW Size	Error
16×16	-1.69%
24×24	-1.96%
32×32	-1.95%
48×48	-1.82%
64×64	-1.99%
96×96	-1.91%
128×128	-1.81%
256×256	-2.04%

Fig. 4.11: Velocity profiles with different sizes of IW. Dashed line represents the limit of integration. (a) - 16 × 16, (b) - 32 × 32, (c) - 64 × 64, (d) - 128 × 128).
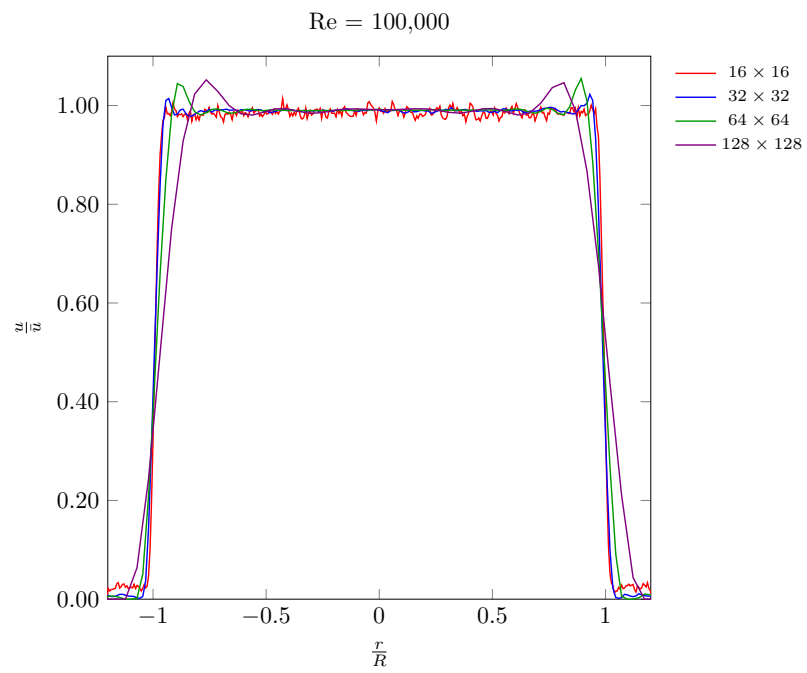
Fig. 4.12: Velocity profiles for different IW sizes.

CHAPTER 5

DISCUSSION

5.1   Spatial Averaging for Two Component Data

Since laser sheets have a finite thickness, 2C PIV data reports velocity averaged over the thickness of that laser sheet. Velocity is 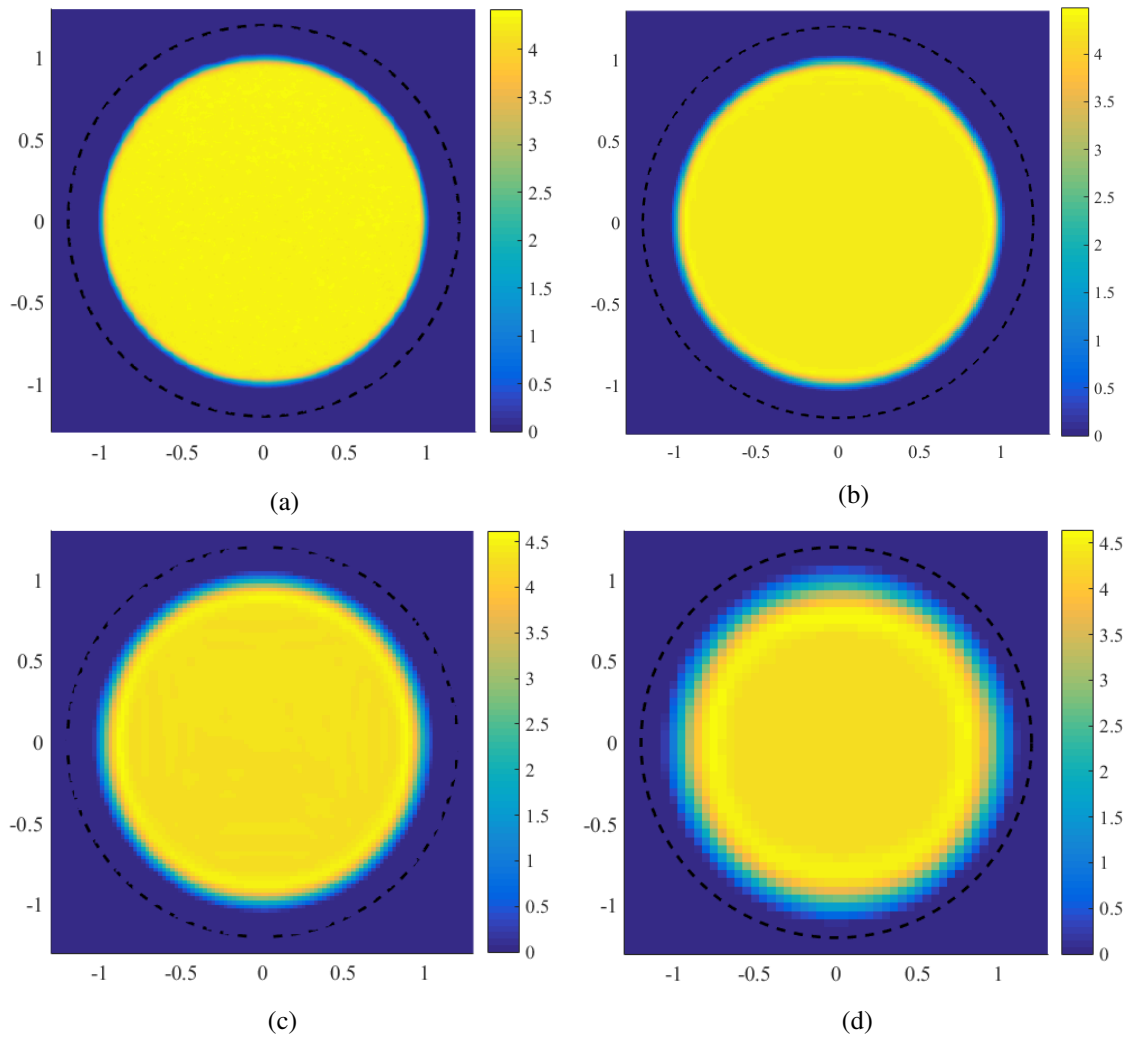a maximum across a line that passes through the exact center of the nozzle, and decreases as you move away from the center which effect is shown in Fig. 5.1. This effect will trend the velocity downward, and thus decrease the measured value of flow rate.

Fig. 5.1: Velocity profiles (red) traversed in the $-y$ direction across the nozzle exit. Each velocity profile represents the velocity on the corresponding dashed black line. This shows that averaging over a finite thickness would trend the velocity downward, particularly near the walls.

A study was done to see the magnitude of the effect of averaging over the thickness of the laser sheet. This was done by using stereo PIV data and averaging over a span of an increasing amount of vectors. The results of this study are shown in Fig. 5.2. With a laser sheet thickne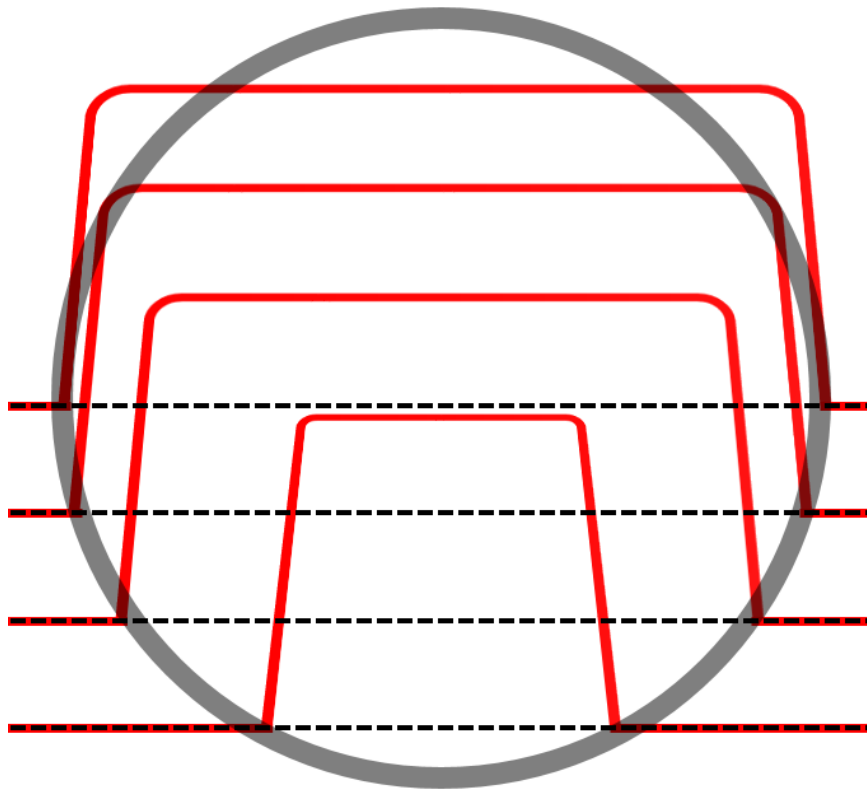ss of 0.6mm used in this experiment, an increase in error of approximately 0.1% can be expected, which is considered insignificant.

5.2 Previous Research

All successful cases, Stereo and 2C, produced approximately -2% volume flow rate error. These results are consistent with that of Cressall [1], whose results for a rectangular nozzle are shown in Table 5.1.

The consistency of these results suggests one of two things: either there is an inherent error in the methods of measurement using PIV, or the flow meter used for this project has a calibration error. We deem the former unlikely due to the large number of independent measurements in this work and that of Cressall that agree.

5.3 Impact of Pre-Processing

As was previously discussed, pre-processing is an attempt to increase the signal-to-noise ratio. This is generally done by seeking to remove any object in the image that is not a particle. When reviewing preliminary data taken in during shakedown, it was noticed that there were two small irregularities in the flow near 5 and 7 o'clock on the nozzle. These small defects were originally thought to be physical features in the flow, and unavoidable.

After closer inspection of the raw images, small reflections of the laser were present on the inner edge of the nozzle surface. With no preprocessing, the PIV algorithm can only recognize these reflections as static particles, which biases the velocities in those areas to zero. The difference in final results can be seen in Fig. 5.3.

5.4 Bias due to Calibration Target

After data were acquired, it was discovered that the calibration target did not match nominal dimension for the plane-to-plane depth $(\delta_p,$ Fig. 5.4) of 1.00mm. The value measured was 1.03mm
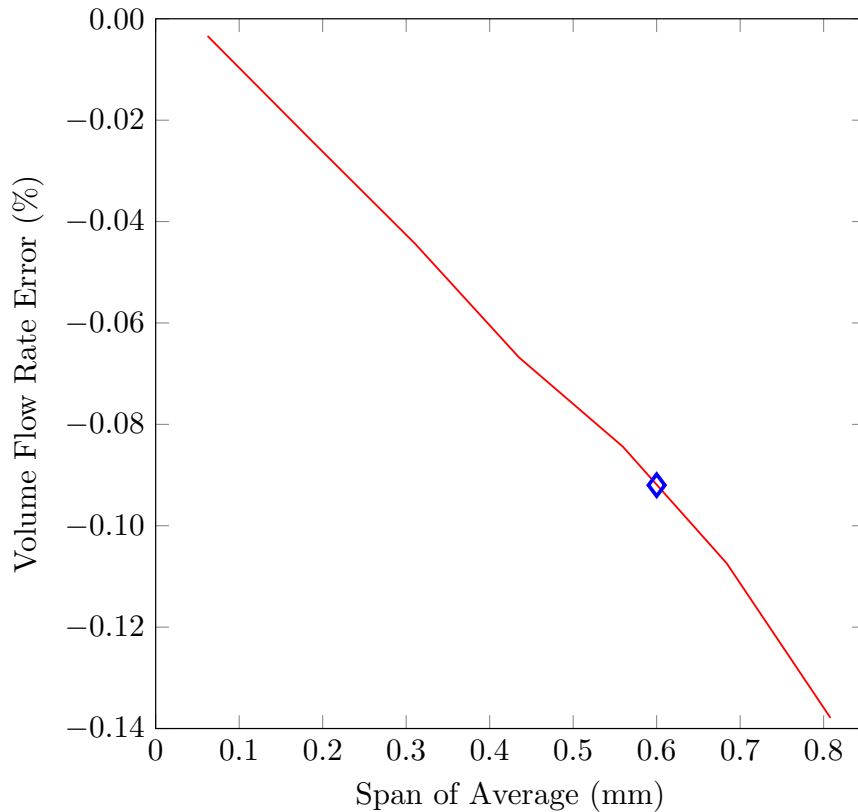
Fig. 5.2: The effect on volume flow rate error of averaging over the thickness of the laser sheet. The diamond represents the laser sheet thickness of this experiment.

Table 5.1: Volume flow rate error from Stereo PIV for different Reynolds Number for rectangular nozzle.

Reynolds Number	10,000	75,000	100,000
Error (%)	-1.58%	-2.03%	-2.08%

or 3% larger than the reported value and outside of the manufacturer's specification of $\pm$ 0.01mm. When this value was changed in calibration procedure, the resulting centerline velocity magnitude of the flow rate error decreased by approximately the same 3%.

This measurement is generally not a major concern because the through-plane velocity component is often more of a secondary priority. However, when trying to measure volume flow rate with Stereo PIV, the through-component is the primary measurement and thus the (δ_p) must be known to a high accuracy. We suggest that the user measure this distance as accurately as possible since this is likely the largest bias error in this measurement.

Measurements were made across the span of the calibration target in several locations with a Mitutoyo Height Master, which is accurate to 0.00001", and it was determined that δ_p for the calibration target used for this project was on average 1.03mm. The error for velocity caused by the 3% error in the calibration target is shown in Fig. 5.5, any differences between the two profiles translates directly to an underestimation in flow rate.

It was found that for Stereo PIV, the plane-to-plane depth on the calibration plate was a crucial value to know with a high degree of accuracy. This matters because the bulk direction of the flow is in this direction, and calibration in the flow direction is directly correlated to the calibration in the same direction.

(a)   (b)
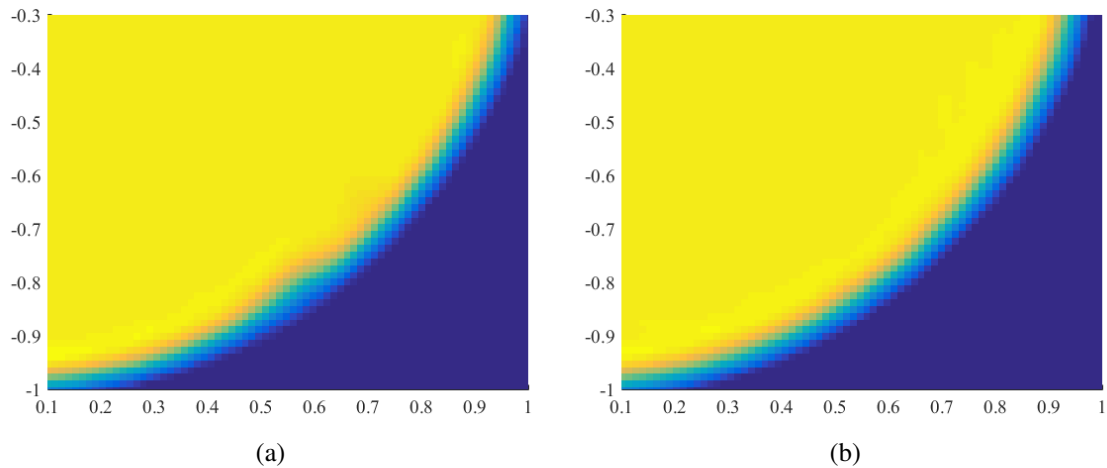
Fig. 5.3: Contour plots of velocity for raw (a) and Pre-processed (b) data for camera angle of $45°$ and Re $= 100,000$.
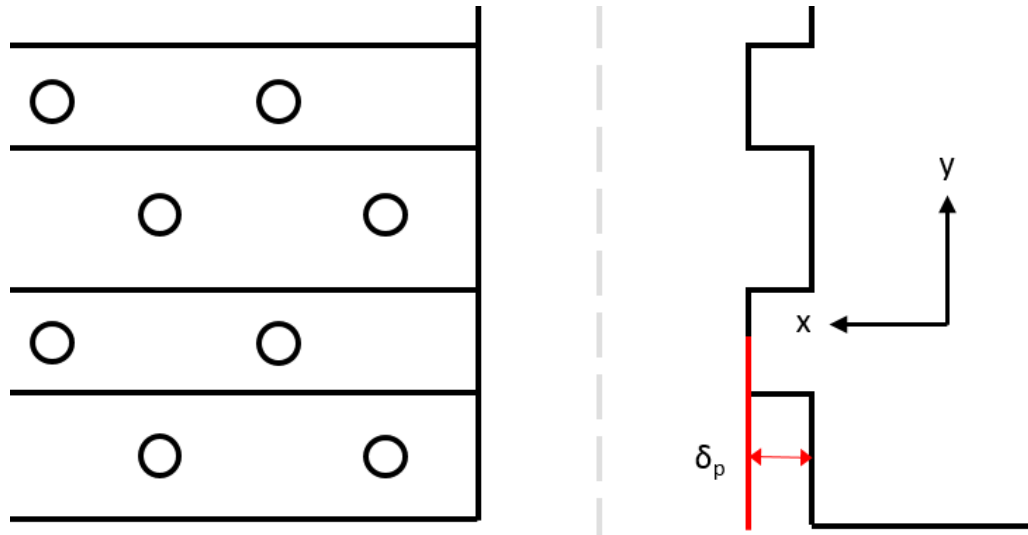
Fig. 5.4: Location of plane-to-plane measurement for which a discrepancy was found between the specified value and as-built.
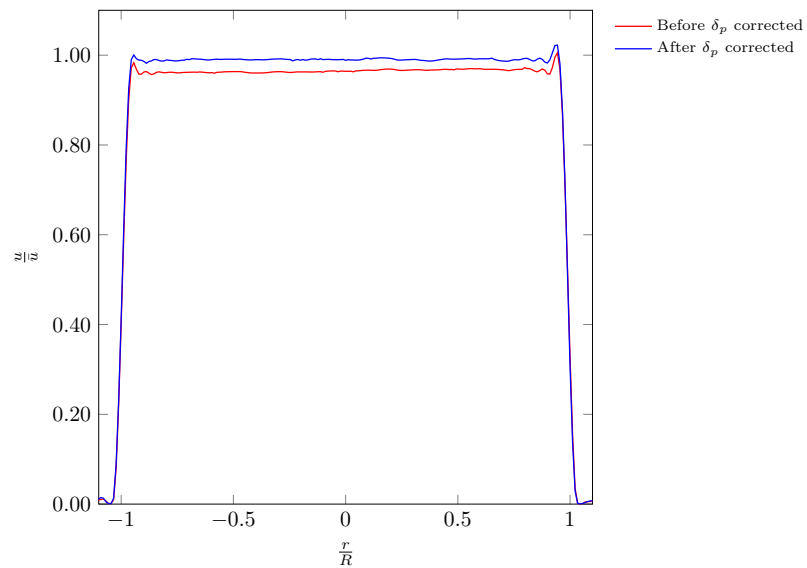

Fig. 5.5: Velocity profiles for before and after δ_p was corrected. The velocities in the core are 3% different.

CHAPTER 6

CONCLUSION

The goals of this work were to assess the impact of spatial resolution, preprocessing, calibration plate accuracy, and laser sheet thickness on measuring volume flow rate through a round nozzle using both 2C PIV and stereo PIV. The effects of these parameters were examined by evaluating the volume flow rate deviation when compared to an accurate flowmeter and centerline velocity profiles of the nozzle.

Two component and Stereo PIV each have advantages and disadvantages. Two component data only requires a short amount of set up and processing time. The main disadvantage of 2C is that we only have velocity information on one line across the nozzle exit. For the present work, we determined that the flow was symmetric across the entire nozzle, but this is not always true, and features not common to the whole exit cannot be captured when using 2C PIV.

When compared to 2C, Stereo PIV requires longer set up time in addition to a longer time to process the data. In contrast to 2C, Stereo acquires data across the entire nozzle exit; therefore any unexpected features in the flow can be captured.

Careful analysis revealed a defect in the calibration target, and the 3% error in δ_p translated to the same magnitude in flow rate underestimation. We conclude that, when using through-plane SPIV, the accuracy of the volume flow rate cannot be any better than the accuracy of the depth of the calibration target.

Other parameters that were tested included IW size, Reynolds Number, and angle of acquisition for stereo PIV. No clear trends were observed for any of these parameters. Flow rate errors were expected to increase with IW size, but this study shows that the measurements is not affected as long as the limits of integration are loosely fitted to the geometry of interest. Higher Reynolds number flows have more shear which generate large errors in PIV, but this work showed almost no difference in flow rate error. Stereo measurements are acquired with two cameras viewing the measurement plane at an angle. The through plane component of velocity has been reported to be sensitive to

this angle [5], but our work did not show any trends for camera angle. Preprocessing is required to remove reflections that bias velocity values to zero.

REFERENCES

[1] Cressall, R., *Best Practices For Volume Flow Rate Measurements Using PIV At The Exit Of A Turbulent Planar Jet*, Master's Thesis, Utah State University, 2016.

[2] Pope, S. B., *Turbulent Flows*, Cambridge University Press, 2015.

[3] Lozanova, M. and Stankov, P., "Experimental investigation on the similarity of a 3D rectangular turbulent jet," *Experiments in Fluids*, Vol. 24, 1998, pp. 470–478. doi:10.1016/s0017-9310(03)00155-8.

[4] Prasad, A. K., "Stereoscopic particle image velocimetry," *Experiments in Fluids*, Vol. 29, Feb 2000, pp. 103–116.

[5] Adrian, R. J. and Westerweel, J., *Particle Image Velocimetry*, Cambridge University Press, New York, New York, 1st ed., 2011.

[6] Keane, R. D. and J., A. R., "Theory of cross-correlation analysis of PIV images," *Applied Scientific Research*, Vol. 49, July 1992, pp. 191–215.

[7] Timmins, B. H., *Automatic Particle Image Velocimetry Uncertainty Quantification*, Master's Thesis, Utah State University, 2011.

[8] LaVision GmbH, *FlowMaster Product Manual, Item Number: 1105011-4*, LaVision GmbH, Anna-Vandenhoeck-Ring 19, D-37081 Göttingen, Germany, Mar 2015.

[9] LaVision GmbH, *DaVis 8.3 Software Manual, Item Number: 1105xxx*, LaVision GmbH, Anna-Vandenhoeck-Ring 19, D-37081 Göttingen, Germany, Mar 2015.

[10] Scarano, F. and Sciacchitano, A., *Robust Elimination of Light Reflections in PIV*, s.n., 2011, pp. 1–7.

[11] Willert, C., "Stereoscopic digital particle image velocimetry for application in wind tunnel flows," *Measurement Science and Technology*, Vol. 8, No. 12, 1997, pp. 1465.

[12] Wieneke, B., "Stereo-PIV using self-calibration on particle images," *Experiments in Fluids*, Vol. 39, No. 2, 2005, pp. 267–280. doi:10.1007/s00348-005-0962-z.

[13] Kähler, C. J., Astarita, T., Vlachos, P. P., Sakakibara, J., Hain, R., Discetti, S., La Foy, R., and Cierpka, C., "Main results of the 4th International PIV Challenge," *Experiments in Fluids*, Vol. 57, No. 6, 2016, pp. 97. doi:10.1007/s00348-016-2173-1.

[14] van Doorne, C. W. H. and Westerweel, J., "Measurement of laminar, transitional and turbulent pipe flow using Stereoscopic-PIV," *Experiments in Fluids*, Vol. 42, No. 2, 2007, pp. 259–279. doi:10.1007/s00348-006-0235-5.

[15] Westerweel, J., "Fundamentals of digital particle image velocimetry," *Measurement Science and Technology*, Vol. 8, No. 12, 1997, pp. 1379.

[16] Lecordier, B., Demare, D., Vervisch, L. M. J., Réveillon, J., and Trinité, M., "Estimation of the accuracy of PIV treatments for turbulent flow studies by direct numerical simulation of multi-phase flow," *Measurement Science and Technology*, Vol. 12, No. 9, 2001, pp. 1382.

[17] Sciacchitano, A., Neal, D. R., Smith, B. L., Warner, S. O., Vlachos, P. P., Wieneke, B., and Scarano, F., "Collaborative Framework for PIV Uncertainty Quantification: Comparative Assessment of Methods," *Measurement Science and Technology*, Vol. 26, No. 7, 2015, pp. 1–15. doi:10.1088/0957-0233/26/7/074004.

[18] Coleman, H. W. and Steele, W. G., *Experimentation, Validation, and Uncertainty Analysis for Engineers*, John Wiley and Sons, Hoboken, NJ, 3rd ed., 2009.